Transverse dynamics of a relativistic electron beam in an underdense plasma channel

Andrew A. Geraci and David H. Whittum
Stanford Linear Accelerator Center, Stanford University, Stanford, California 94309

(Received 11 January 2000; accepted 11 April 2000)

The transverse dynamics of a relativistic electron beam in a plasma less dense than the beam is analyzed, with particular attention to the electron-hose instability as it appears in a plasma channel of finite radius. A comparison is made between analytic asymptotic forms, linearized ''beam break-up'' simulations, and particle-in-cell simulations. The analysis provides a framework for the interpretation of projected and time-resolved diagnostics in such a system. Examples used for illustration correspond to parameters of an experiment in progress, employing a 30 GeV electron beam in a 1.5 m plasma cell, with the amplification of beam-centroid offsets on the order of $10^0-10^2\times$, depending on experimental settings. © *2000 American Institute of Physics.* [S1070-664X(00)04907-7]

I. INTRODUCTION

In recent times the subject of relativistic electron beam propagation in plasma has blossomed into an extensive field of research, much of it centered on the *plasma wakefield accelerator* (PWFA).[1] The PWFA makes use of an intense electron beam propagating through a plasma to induce a plasma oscillation trailing the beam. The large longitudinal electric field associated with this plasma oscillation may someday power a TeV electron accelerator. As yet it is too soon to determine whether the PWFA will live up to its promise. One reason for this is *transverse instability* of the drive beam. Although this has been the subject of theoretical work,[2] recent experimental work[3,4] motivates a detailed and refined theoretical analysis, including a comprehensive survey of the parameter space for unstable perturbations.

The PWFA in the limit of a plasma more dense than the beam (''overdense'') has been the subject of numerous theoretical[5–9] and experimental studies.[10–12] Some analysis of stability in the overdense regime has also been performed.[13,14] One disadvantage of the overdense PWFA is the inherent nonlinearity of focusing in an overdense plasma. In the limit of a plasma less dense than the beam (''underdense''), fields witnessed by the beam consist of those produced by a relatively motionless channel of ions superimposed on the transient fields associated with a plasma electron population expelled into an annulus surrounding the beam.[15] The uniformity of the accelerating wakefield, and the linearity of the focusing in this regime, have motivated studies of longitudinal wakefields in this limit.[16] While the accelerating gradients achievable in the underdense PWFA appear promising, this system will be vulnerable to breakup of the drive beam, in particular, a transverse two-stream (''electron hose'') instability, that appears in any such uniformly focusing beam-formed channel.[17–20]

In the present work we consider a highly relativistic short bunch, comparable to the plasma period in length, propagating in a dilute, collisionless plasma. The dynamics of the system are governed by the betatron oscillations of the beam, plasma oscillations, and their mutual electrostatic coupling. For a highly relativistic beam, the dominant beam perturbations can be *transverse* rather than *longitudinal*, even for slight deviations from a perfectly aligned round beam, and both focusing and deflection may be expected.

A. Outline

In this work we investigate transverse stability of a short bunch in an underdense plasma. The goal is to provide a formulation suitable for understanding of integrated and time-resolved diagnostics in a PWFA. We focus on quantifying amplification of incoming beam offsets. For illustration we employ parameters as listed in Table I, close to those of an experiment in progress.

In Sec. II we outline an analytic description of the system for small perturbations. A numerical solution of this linear integrodifferential equation (''beam breakup'' equation) is compared to analytic asymptotic forms to illustrate the scalings. Parameters for the plasma and beam correspond to Table I. In Sec. III we examine the same examples, with the help of a particle-in-cell (PIC) simulation, making a comparison between the (nonlinear) PIC simulation and the (linearized) beam breakup simulation. Having gained some confidence in the PIC simulation through a comparison of scalings for the idealized equilibrium, we use the PIC simulation to examine in detail the transient behavior corresponding to Table I. Section IV includes an analysis of an idealized PWFA experiment, providing a theoretical framework to interpret the results, and illustrative output to indicate the phenomena accessible with beam position monitor (BPM) data for the orbit, and beam profile data, both time resolved and projected. Conclusions are offered in Sec. V.

B. Regimes of propagation

It is useful to review at the outset the basic features of relativistic electron beam propagation in plasma. The result

TABLE I. Nominal electron beam and plasma parameters for examples.

Quantity	Symbol	Nominal value
Electrons in bunch	N_b	4×10^{10}
Bunch length	σ_z	0.7 mm
rms, norm emittance	ϵ_{nx}	6×10^{-5} m rad
	ϵ_{ny}	1×10^{-5} m rad
rms beam size	$\sigma_{x,y}$	50 μm
Beam energy	$mc^2\gamma$	30 GeV
Beam density	n_{b0}	1.45×10^{15} cm^{-3}
rms energy spread	σ_δ	3×10^{-3}
Plasma tank length	L_p	1.5 m
Channel radius	R	1 mm
Plasma density	n_p	3×10^{14} cm^{-3}

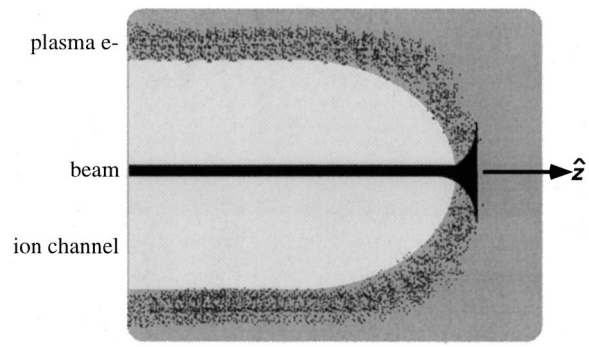

FIG. 1. The radial electric field of the relativistic electron beam expels plasma electrons from a large volume, or ''channel.'' Beam electrons are then focused by the radial electric field of the relatively immobile ions.

is a picture of the equilibrium or ''zeroth-order'' system to which we will consider dipole (centroid) perturbations.

We will consider an injected electron beam traveling in the s direction, described by a Gaussian transverse profile with number density,

$$n_b(x,y,\tau)=n_{b0}(\tau)\exp\left(-\frac{x^2}{2\sigma_x^2}-\frac{y^2}{2\sigma_y^2}\right), \tag{1}$$

where the density on axis is given by

$$n_{b0}(\tau)=\frac{I_b(\tau)}{2\pi\sigma_x\sigma_y c}, \tag{2}$$

with a current waveform given by

$$I_b(\tau)=\frac{Q_b}{(2\pi)^{1/2}\sigma_t}\exp\left(-\frac{\tau^2}{2\sigma_t^2}\right). \tag{3}$$

The ''beam coordinate'' $\tau=t-s/c$, and we approximate the beam drift velocity by c, the speed of light, thereby neglecting radiative effects. The beam charge is Q_b, the rms bunch length is $\sigma_z=\sigma_t c$, and the rms beam dimensions in the transverse plane are σ_x and σ_y. It is convenient to refer to the beam wave number, $k_b=(4\pi n_{b0}r_e)^{1/2}$, where $r_e=e^2/mc^2\approx2.82\times10^{-13}$ cm is the classical electron radius, $-e$ is the electron charge, and m is the electron mass.

There are in general four regimes of propagation, as listed in Table II, and each may be seen in Fig. 1.

When the current waveform rises slowly on the scale of a plasma oscillation, $k_p\sigma_z\gg1$, the beam represents an adiabatic perturbation to the plasma, and the four regimes listed in Table II are clearly evidenced. For the PWFA, we are, in general, interested in a ''short'' pulse, one for which $k_p\sigma_z<1$. In this case the plasma response is transient, and a plasma oscillation trails the drive beam. Here we refer to the plasma wave number $k_p=(4\pi r_e n_p)^{1/2}$. The angular plasma frequency is $\omega_p=k_p c$.

TABLE II. Four regimes of propagation for a relativistic electron beam in a plasma.

Condition	Regime
$n_p<n_b/\gamma^2$	Unfocused
$n_p<n_b$	Ion focused
$n_p>n_b$, $k_p\sigma_{x,y}\leqslant1$	Magnetically self-focused
$n_p>n_b$, $k_p\sigma_{x,y}>1$	Current neutralization

As the beam head propagates through the plasma, it continuously expels some plasma electrons from the beam volume. If the beam density is sufficiently high that $n_{b0}>n_p$ then a region near the beam axis is completely denuded of plasma electrons, forming an ''ion-channel.'' For illustration, consider a ''round beam,'' one with $\sigma_x=\sigma_y=\sigma_r$. One may estimate the radius of the ion channel by considering that the beam and ion electrostatic fields cancel exactly at some radius R_n, the ''neutralization radius,'' satisfying

$$\frac{1}{2}\frac{n_p}{n_{b0}}=\frac{\sigma_r^2}{R_n^2}\left[1-\exp\left(-\frac{1}{2}\frac{R_n^2}{\sigma_r^2}\right)\right].$$

In the limit $n_{b0}/n_p\gg1$, this reduces to $R_n\approx\sigma_r(2n_{b0}/n_p)^{1/2}$. In the limit of adiabatic current rise, $k_p\sigma_z\gg1$, one may picture plasma electrons being adiabatically expelled beyond this radius.

The transverse force witnessed by a beam electron in this ''ion-focused'' regime takes the form,

$$F_r\approx-\tfrac{1}{2}mc^2k_p^2r,$$

where we make use of the approximation $n_p\gg n_b/\gamma^2$, valid for an ultrarelativistic beam. In this regime the beam electric and magnetic field contributions to the transverse force nearly cancel and the ion-pinch force dominates. Transverse motion of a single electron is described by

$$\frac{d}{ds}\gamma\frac{d}{ds}\mathbf{r}_\perp+\gamma k_\beta^2\mathbf{r}_\perp\approx0, \tag{4}$$

where the betatron wave number is determined by the ion density,

$$k_\beta=\frac{k_p}{\sqrt{2\gamma}}. \tag{5}$$

On the other hand, when the plasma is denser than the beam—a condition that always applies for some portion of the beam head—the beam electric field expels only a fraction of the plasma electron charge, enough so that the resulting surfeit of ion charge is adequate to cancel the electric field of the beam. In this limit, the net charge density is approxi-

mately zero, and the only field component remaining is the magnetic field due to the beam. Transverse motion of a single beam electron is again described by Eq. (4), at least, for small displacements from the beam axis, $r \ll \sigma_r$, except that the betatron wave number in this regime is determined by the beam density,

$$k_\beta = \frac{k_b}{\sqrt{2\gamma}}. \tag{6}$$

Notice that as plasma electrons are expelled from the beam volume, they are also accelated backward, at the expense of work done by the beam head. This backward component of the electron motion corresponds to a return current carried by the plasma electrons. A collisionless plasma will oppose the current flow corresponding to an injected electron beam.[21] This return current sheath extends radially with a radial *e*-folding length of k_p^{-1} beyond the ion channel. In the limit $k_p \sigma_{x,y} > 1$, these plasma return currents are flowing through the bulk of the beam, as opposed to a volume much larger than the beam, and in this limit, the net magnetic field within the beam is diminished. In this ''current neutralization'' regime, the net transverse force experienced by the beam is simply its own magnetic field, diminished somewhat by the contribution of the plasma electrons. This regime is accessible when the beam size is large and the current is low.

C. Higher-order effects

A number of higher-order effects should be noted, as they are accessible in principle, depending on the parameter range. Small angle scattering may result in emittance growth,[22] although for beam and plasma parameters considered herein the effect is negligible. Ionization by the beam is of concern in determining the actual axial plasma density profile. Ionization is produced by the beam through electron impact, gas breakdown, stripping of atoms and ions in the strong radial electric field at the beam ''edge,'' or tunneling in the presence of this field.[23,24] In addition, one may expect secondary electron multiplication (breakdown), an effect scaling with E/p, the ratio of radial electric field to pressure.[25] In the meantime, plasma electrons are also lost through recombination.[26,27] For a short, picosecond electron pulse and working gas pressures in the range of mtorr, ionization processes are relatively slow, and recombination is negligible during the beam transit. The time scale for the massive ions to collapse inward and neutralize the beam charge is large compared with times of interest, and ion motion can be neglected. Finally, the approximation of a collisionless plasma is fair; however, in the collisionless limit, instabilities may replace collisions in dissipating the wakefield. The formation of the accelerating wakefield requires a backward acceleration of plasma electrons, and this flow is subject to the two-stream (Buneman) instability coupling the plasma electron motion to the ions. For a lithium plasma with density as in Table I, the time scale of the damping is several plasma periods, and this effect is negligible for the short drive bunch we consider.

II. LINEARIZED DYNAMICS

We consider beam centroid evolution in the limit of an underdense plasma. The problem is analytically tractable in the limit of a preformed ion channel, for in this limit the beam and plasma constitute an equilibrium. Convenient approximations include the neglect of ion motion, large plasma skin depth, and adiabatic current variation.[17] The evolution of the beam centroid, ξ, in beamline coordinate s and beam coordinate τ is described by a ''beam breakup'' equation,[17]

$$\left(\frac{\partial}{\partial s}\gamma\frac{\partial}{\partial s}+\gamma k_\beta^2\right)\xi(s,\tau)=\int_0^\tau W(\tau-\tau')\xi(s,\tau')d\tau', \tag{7}$$

where the wakefield is

$$W(\tau)=\frac{\omega_0^3}{c^2}\sin(\omega_0\tau), \tag{8}$$

k_β is the betatron wave number, and $\omega_0=\omega_p/\sqrt{2}$.

With the assumption of adiabatic current rise, i.e., $k_p\sigma_z \gg 1$, the form of the beam breakup equation is independent of the beam current profile. At higher currents, the channel radius adiabatically expands, diminishing the electrostatic field seen by the beam. This geometrical expansion compensates for the higher current, leaving the drive term in Eq. (7) independent of beam current.

This integrodifferential equation defines a special function $\xi(s,\tau)$ for each choice of initial conditions,

$$\xi_0(\tau)=\xi(s=0,\tau), \quad \xi_0'(\tau)=\frac{\partial\xi}{\partial s}(s=0,\tau).$$

For the sake of illustration we will consider initial conditions of the form

$$\xi_0(\tau)=\xi_0+\dot{\xi}_0\tau, \quad \xi_0'(\tau)=0.$$

The precise evolution of the beam centroid may be determined by numerical solution, breaking the integral in Eq. (7) over τ' into a discrete sum. Alternatively, the result may be determined up to quadrature in terms of an inverse Laplace transform. The resulting integral is amenable to a steepest descents calculation, tractable in certain limiting cases.

In the following we summarize these asymptotic results, and a comparison with the ''exact'' numerical result, using for illustration a plasma density, plasma length, and beam energy as in Table I.

In the limit of a weak focusing and a long bunch, with a uniform initial offset, $\dot{\xi}_0=0$, one finds[17]

$$\xi(s,\tau)\approx 0.202\xi_0\frac{A^{1/2}}{\omega_0\tau}e^A\sin\left(\omega_0\tau-\frac{A}{\sqrt{3}}-\frac{\pi}{12}\right), \tag{9}$$

with an exponent given by

$$A(s,\tau)=\frac{3^{3/2}}{4}[(k_\beta s)^2(\omega_0\tau)]^{1/3}, \tag{10}$$

where the conditions $\omega_0\tau \gg A \gg 1$ and $k_\beta L_g \ll 1$ are assumed.

In the limit of strong focusing and a short bunch, the asymptotic form with a uniform initial offset is[18]

$$\xi(s,\tau)\approx 0.263\frac{\xi_0}{A^{1/2}}e^A\cos\left(k_\beta s-\frac{A}{\sqrt{3}}+\frac{\pi}{12}\right), \tag{11}$$

where

$$A(s,\tau)=\frac{3^{3/2}}{4}[(k_\beta s)(\omega_0\tau)^2]^{1/3}. \tag{12}$$

Here it is assumed that $k_\beta s \gg \omega_0\tau$ and $\omega_0\tau<1$.

For a tilted initial offset, $\xi_0=0$, the asymptotic form is modified to

$$\xi(s,\tau)\approx 0.341\frac{\dot{\xi}_0\tau}{A^{3/2}}e^A\cos\left(k_\beta s-\frac{A}{\sqrt{3}}+\frac{\pi}{4}\right). \tag{13}$$

The large plasma skin-depth approximation can be cast in the form $k_p b \ll 1$, where b is the plasma neutralization radius. In the adiabatic approximation, $b^2=a^2(n_b/n_e)$, where $a=\sqrt{2}\sigma_{x,y}$, the effective beam radius. The effect of smaller plasma skin depth (larger $k_p b$) on the wakefield in Eq. (8) can be quantified[28] as

$$W_{\text{eff}}(\tau)=W\left[1-\left(\frac{k_p b}{4}\right)^2\right]. \tag{14}$$

In the short-bunch, strong-focusing asymptotic limit the growth factor in the exponential of Eq. (12) is reduced to

$$A_{\text{eff}}=A\left[1-\left(\frac{k_p b}{4}\right)^2\right]^{1/3}. \tag{15}$$

The wakefield in Eq. (8) is derived for an infinite plasma and is reduced from the effect of the finite plasma outer radius. The linearized beam breakup (BBU) wakefield due to an annular plasma sheath has been calculated[29] and the modification to Eq. (8) can be determined for finite outer plasma radius. Rewriting Eq. (8) as

$$W(\tau)=W_0\sin(\omega_0\tau) \tag{16}$$

and letting α be the ratio of outer annulus radius to b, the inner neutralization radius, the wake is modified to

$$W_0\left\{\sin(\omega_0\tau)\cos[\omega_0\tau/(2\alpha)] + \frac{1}{2\alpha}\sin[\omega_0\tau/(2\alpha)]\cos(\omega_0\tau)\right\},$$

neglecting terms of order $1/\alpha^2$. For parameters in Table I, $\alpha\approx 10$, and the infinite plasma wakefield in Eq. (8) is a good (within a few percent) approximation for bunch lengths we consider, satisfying $\omega_0\tau<2\pi$.

For illustration, the result of Eq. (11) is compared to the numerical solution of Eq. (7) in Fig. 2 for nominal parameters. The numerical solution of Eq. (7) is obtained by a macroparticle (MAC) code employing a fourth-order Runge–Kutta scheme. The result indicates a tail centroid offset amplification on the order of six times for an initially uniformly offset beam and a bunch length of 0.6 mm. For a ''tilted'' initial offset, the amplification is ≈ 2 times. For a smaller plasma density of $2\times 10^{14}\,\text{cm}^{-3}$ there is a reduction in transverse growth from 6 to ≈ 3 times for a horizontal initial offset. This $3\times$ growth is in turn reduced to approximately $1.3\times$ for a ''tilted'' offset. For plasma and beam density as in Table I, the wake is only slightly reduced according to Eq. (14), by $\approx 1.5\%$. This in turn causes only a minor reduction in growth by approximately 6% in the examples involving this plasma density.

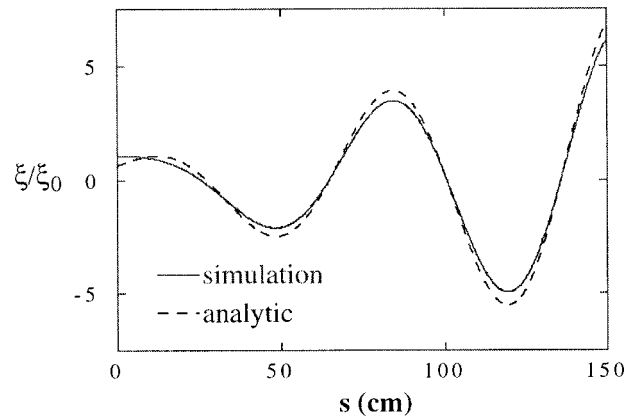

FIG. 2. A comparison of the beam tail centroid versus axial displacement through the plasma from the numerical solution of Eq. (7) (solid), and the asymptotic form of Eq. (11) (dashed) for bunch length 0.6 mm and plasma density, beam energy, plasma length as in Table I.

III. PIC SIMULATION STUDIES

The linearized model for BBU, Eq. (7) is helpful in that it provides a direct, fast means of determining growth. However, it makes a number of approximations that require further assessment. Given the transient and potentially nonlinear behavior of the plasma, the most accurate means of determining the evolution of the system is the particle-in-cell simulation. While fully electromagnetic models are in use,[4] they require exorbitant amounts of simulation time, limiting their usefulness, particularly for the dipole problem. Moreover, they include too much extraneous dynamics, as the full Maxwell's equations are not required for this magnetoinductive problem. In fact, in the limit of large plasma skin depth, the problem becomes one of magnetostaties and electrostatics. We discuss next a simulation code we have developed that is appropriate for this regime, first discussed in Ref. 20. We are particularly interested in assessing the less idealized circumstances to be found in the experiment, transient channel formation and nonadiabatic current variation.

The PIC simulation divides the beam into $N_t\approx 30\times(\omega_p\tau/2\pi)$ slices, and each beam slice is modeled by $N\approx 4096-16\,384$ macroparticles. Each slice is initialized at $s=0$ with a predetermined distribution, either Gaussian or Kapchinskij–Vladimirskij (K–V), making use of symmetrized Hammersley deviates. The K–V distribution is defined in Ref. 30. The beam particle motion in transverse position $\mathbf{r}_\perp$ and momentum $\mathbf{p}_\perp$ (normalized by mc) is governed by the pinch gradient, ψ,

$$\frac{d\mathbf{r}_\perp}{ds}=\frac{\mathbf{p}_\perp}{p_s},\quad \frac{d\mathbf{p}_\perp}{ds}=-\nabla_\perp\psi,$$

and these equations are advanced in s by a leapfrog algorithm, holding constant axial momentum p_s (normalized by mc), and permitting no slippage in τ.

The pinch potential $\psi = A - \phi$, where the axial magnetic and electrostatic potentials are determined from the reduced Maxwell's equations, expressed in terms of the beam charge density ρ_b, the plasma–electron charge density ρ_e, and the fixed ion charge density ρ_i,

$$\nabla_\perp^2 \phi = -\frac{4\pi e}{mc^2}(\rho_b + \rho_e + \rho_i),$$

$$\nabla_\perp^2 A = -\frac{4\pi e}{mc^2}\rho_b .$$

These are solved by a fast Fourier transform in x and y, with periodic boundary conditions. Charge allocation and field interpolation are performed by area weighting in $x-y$.

As for the plasma electrons, one ''slice'' of $M \approx 65\,536-131\,072$ plasma macroparticles is initialized for each step in s, and passed through the beam from the head to the tail. The plasma initialization loads $M/2$ pairs (x,y) uniformly within the unit circle, by rejection, and quiets the loading by reflection through the origin. Plasma particle momenta were initialized to zero. The plasma advance is a leapfrog in the beam coordinate τ, governed solely by the electrostatic potential,

$$\frac{d\mathbf{r}_\perp}{c\,d\tau} = \mathbf{p}_\perp , \quad \frac{d\mathbf{p}_\perp}{c\,d\tau} = \boldsymbol{\nabla}_\perp \phi .$$

The sensitivity of results to numerical parameters was gauged by varying the size of the mesh, the number of beam and plasma macroparticles, the integration time step in both s and τ, the distance between the plasma and the boundary, and an offset of the plasma center with respect to the mesh center. As a means to further validate the PIC simulation, it is worthwhile to consider beam propagation in an equilibrated plasma channel. This limiting case can allow for a direct comparison between the PIC results and the numerical solutions of Eq. (7). Where an equilibrated plasma channel is employed, the initial quasineutral equilibrium is achieved by adiabatic relaxation of the initially uniform plasma in the potential of an undisplaced beam. Typical beam displacements are $10^{-5}-10^{-4}$ beam radii, small enough to observe saturation prior to nonlinearity, and large enough to avoid roundoff error.

A. Zeroth-order optics

The first and dominant feature of PIC studies is the envelope evolution of the beam. In general, focusing forces are transient, varying with the beam coordinate τ. In the first approximation, however, one may attempt to gauge the behavior to be expected considering the steady-state results. In this case, the optics are described by Eq. (4), with k_β given by Eq. (5). To describe the beam evolution in this limit, one may employ single-particle tracking, as in a thick lens, or one may employ the envelope equation,

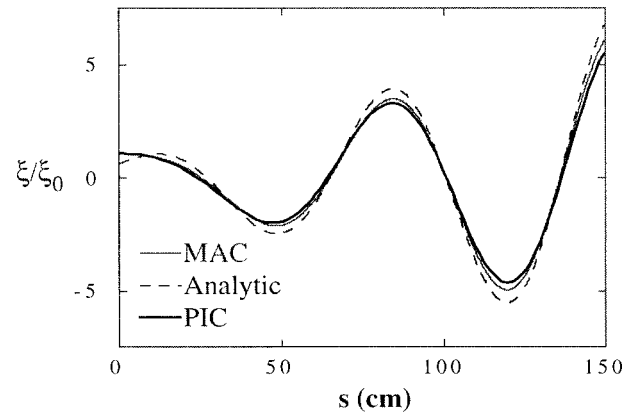

FIG. 3. A comparison of the PIC, MAC, and asymptotic form, for a short-pulse, strong-focusing example, with a top-hat current profile, K–V beam profile, a uniform offset, in an equilibrated channel. The bunch length is $l_b = 0.6$ mm, and the initial offset is $10^{-4} \times a$, where a is the effective beam radius.

$$\frac{d^2\sigma_x}{ds^2} + k_\beta^2 \sigma_x = \frac{\epsilon_x^2}{\sigma_x^3}, \tag{17}$$

and similarly for y. The quantity ϵ_x is the rms emittance, and $\sigma_x^2 = \langle x^2 \rangle - \langle x \rangle^2$. To solve numerically for the beam size, one needs only the beam spot size specified at $s=0$, together with the initial Twiss parameters, β and $\alpha = -\beta'/2$. These quantities then fix the initial conditions on the envelope, $\sigma_x = \sqrt{\epsilon_x \beta_x}$ and $\sigma_x' = -\alpha_x \sigma_x / \beta_x$.

As we will see, the figures of Table I do not correspond to a matched beam, as emittances are $\approx 100\times$ smaller than necessary for matching to the plasma channel for these initial beam dimensions. In the following we will consider two kinds of examples, one as in Table I, and the other ''matched'' with emittance larger than in Table I. The latter examples facilitate a direct comparison with the linearized model (which does not take account of scalloping).

B. Equilibrated plasma

In this section we compare the PIC, linearized model, and analytic results for the strong-focusing, short-bunch regime in an equilibrated plasma channel. Figure 3 shows transverse displacement of the beam tail centroid versus distance though the plasma, as calculated for a uniformly offset bunch by the analytic form, MAC, and PIC. Parameters are as in Fig. 2, and the emittance is matched to the channel to allow a comparison with the linearized MAC code. The initial offset is given in terms of the effective beam radius a, where for a Gaussian beam we set $a = \sqrt{2}\sigma_r$. Figure 4 compares the asymptotic result of Eq. (13) with MAC and PIC results for a tilted initial offset, with parameters as in Fig. 3. For both tilted and uniform initial offset, we observe good agreement between the MAC, PIC, and analytic results. The MAC and analytic results for an equilibrated channel are formulated for a top-hat profile electron bunch. In order to roughly apply MAC or analytic scaling results to a Gaussian electron bunch, a provision must be made to translate the Gaussian longitudinal distribution into an effective top-hat bunch length. The actual Gaussian pulse indicated in Table I

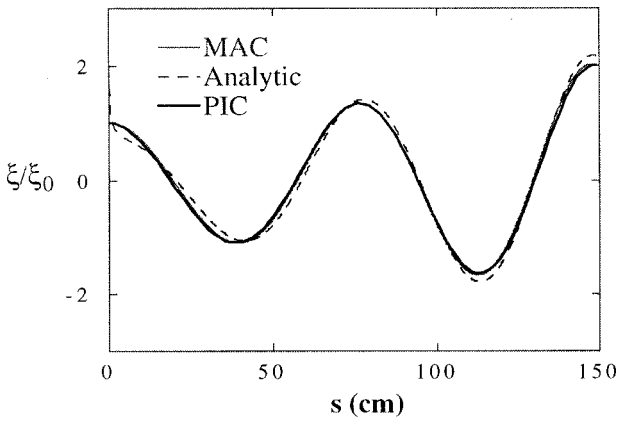

FIG. 4. A comparison of the PIC, MAC, and asymptotic form, for the example of Fig. 3, but with a ''tilted'' initial offset.

corresponds to a bunch length longer than $l_b = 0.6$ mm, indicated in the examples of Figs. 3 and 4. The effective bunch length suitable for a comparison of top-hat and Gaussian current profiles may be determined roughly from the condition $n_{b0} = n_p$, the threshold for the ion-focused regime. This corresponds an effective bunch length $l_b \approx (8\lambda)^{1/2}\sigma_z$, where $\lambda = \ln[n_{b0}(0)/n_p]$. This results in a figure $l_b = 2.67$ mm for Table I, parameters. Results for this longer pulse example are seen in Fig. 5, showing good agreement between the MAC and PIC codes. Other parameters remain as in Figs. 3, 4. Since growth increases by nearly two orders of magnitude for this longer bunch example, the initial offset was reduced from 10^{-4}–10^{-5} beam radii to avoid nonlinearity.

C. Uniform plasma

For the longer bunch example ($l_b = 2.67$ mm), a ''tilted'' initial profile, and a uniform plasma not equilibrated to the beam, results are seen in Fig. 6. Agreement is fair, although the PIC indicated more growth for the uniform case. This may be attributed to the fact that in the uniform case, the beam witnesses plasma electrons at closer proximity for a longer duration, contributing to enhanced wakefields. A competing effect is that the head of the beam has to be ''used up'' to blow out the plasma electrons in the uniform case. It appears that for this particular example the former effect is greater.

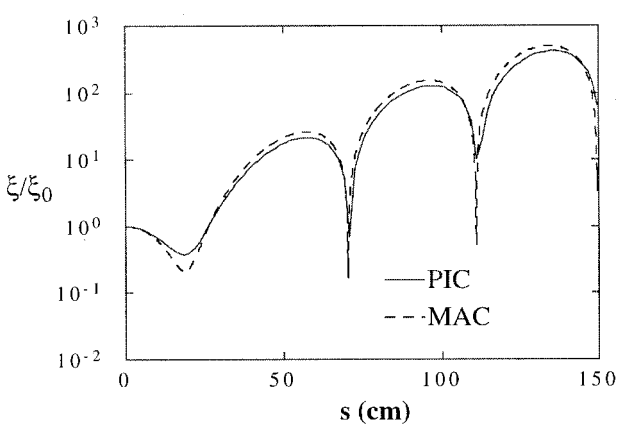

FIG. 5. A comparison of the PIC, MAC for a long-bunch, strong-focusing example, with a top-hat current profile, a uniform initial offset, and an equilibrated channel. Pulse length $l_b = 2.67$ mm.

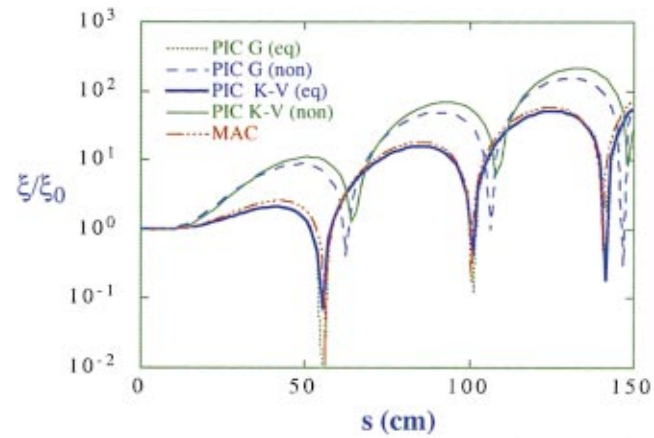

FIG. 6. (Color) A comparison of the PIC, MAC for a longer-bunch, strong-focusing example, with a ''tilted'' initial offset, and an equilibrated channel. The three curves are almost indistinguishable. Also shown is the PIC result for the same parameters, and a uniform plasma channel.

Examples were considered for both Gaussian and K–V transverse beam profiles, and emittance is taken as in Fig. 5. There is no remarkable dependence of tail centroid trajectory on the transverse beam profile in the equilibrated case. This is understandable, since the preformed equilibrated channel has plasma electrons expelled radially beyond the beam volume, and the interaction of the beam and plasma electrons takes place from a distance. In the uniform case, there is $\approx 1.5\times$ less growth for the Gaussian spatial distribution than for the K–V. We attribute this to the fact that the tails of the Gaussian distribution can extend into regions beyond the ion channel and cause phase mixing that may result in reduced growth as compared with the K–V example.

D. Gaussian current waveform

As a more realistic means to gauge the transient behavior associated with beam propagation through uniform plasma, a Gaussian current waveform, Eq. (3), was substituted for the previously considered step bunch of effective length l_b. Figure 7 shows the centroid offset ζ versus beam

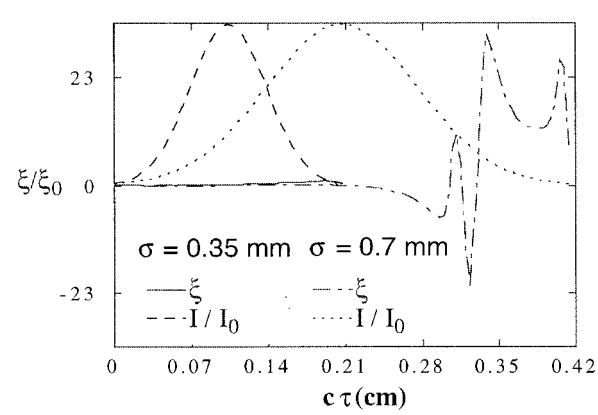

FIG. 7. The PIC result for a centroid offset versus beam coordinate immediately downstream of plasma.

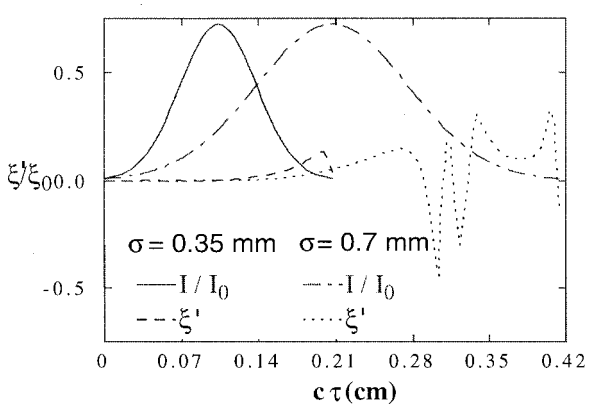

FIG. 8. The PIC result for a centroid exit angle versus beam coordinate immediately downstream of plasma.

coordinate τ at the exit of the plasma for the Gaussian current profile case with a tilted offset for two bunch lengths. Beam current versus τ is shown for reference. Emittance is taken as in Table I. The initial offset of the $3\sigma_z$ tail is normalized to unity on the vertical axis. The $-3\sigma_z$ beam head is defined as zero offset. A case is shown for initial $3\sigma_z$ tail offset of $0.3\times a$, where the beam radius $a=\sqrt{2}\sigma_{x,y}$. Cases calculated for smaller offsets of 0.1 and $0.001\times a$ indicate that the scaling of ξ/ξ_0 is only slightly nonlinear. For the nominal parameters in Table I, the beam tail undergoes significant distortion and amplification of tail centroid offset is in the range of 25–40×. By reducing the bunch length by a factor of 2, so that from head to tail the bunch length is approximately equal to one plasma period, we see a significant reduction in centroid-offset amplification.

The transverse centroid exit angle corresponding to Fig. 7 versus beam coordinate is displayed in Fig. 8. The vertical axis is normalized to the initial displacement in cm of the $3\sigma_z$ beam tail. For example, the figure indicates a $2\sigma_z$ tail deflection of ≈0.6 cm after drifting a distance of 10 m. In contrast, at this plasma density, a purely betatron (no hosing wakefield) deflection of the head–tail offset could, at most, deflect this section of the tail ≈0.1 cm at the same distance.

Figure 9 shows a time-resolved beam projection for parameters as in Table I, with head–tail tilt as in Fig. 7. The horizontal and vertical scales are 4.2 and 1.5 mm, respectively. This head–tail tilt is distorted and amplified by the 1.5 m plasma, as evidenced in Fig. 10. As Fig. 10 indicates, the head of the beam (from ≈0 to 1 mm) undergoes scalloping as an ion channel is formed. The portion of the beam from 1 to 3 mm experiences a channel absent plasma electrons, and is subject to the electron-hose instability. The latter portion of the bunch, after approximately 3 mm, witnesses the collapse of the ion channel and the plasma electron density on axis reaching approximately four times its initial value, causing strong deflection and defocusing.

This wakefield amplification can be significantly reduced by decreasing the bunch length, as indicated by Eq. (13). We consider an example with peak beam current density and other parameters as in Table I, except σ_z is reduced to one-half its original value. With these parameters the bunch length from $\pm 3\sigma_z$ is reduced to approximately one plasma period. As Fig. 11 indicates, the effect of the electron-hose instability is reduced. The beam tail passes through the plasma before the plasma electrons blown out by the head of the beam can collapse inward and the strong defocusing and deflection observed in Fig. 10 are absent. The condition for the beam tail to avoid the plasma channel collapse as observed in the PIC simulation can be cast roughly in the form $k_p\sigma_z<1$.

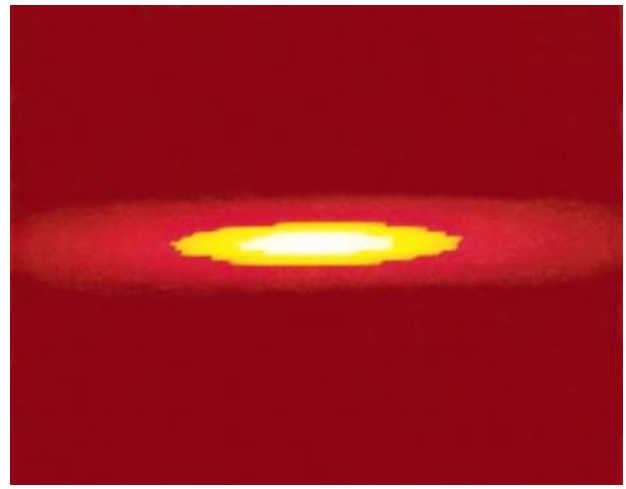

FIG. 9. (Color) Incoming beam profile with head–tail ''tilt.'' The vertical dimension is 1.5 mm; the horizontal 4.2 mm.

In practice, it is difficult to obtain beams with σ_z as small as indicated in Fig. 11. Alternatively, transverse growth can be controlled by reducing the plasma density at fixed σ_z. For plasma density one-fourth its value in Table I (plasma frequency reduced by one-half) and the full σ_z, we maintain the condition that from $\pm 3\sigma_z$ the bunch length is approximately one plasma period. In this case the downstream result is shown in Fig. 12. Focusing is reduced due to lower plasma density, and distortion of the beam tail is absent.

The effect of reducing bunch charge by one-half is shown in Fig. 13. In contrast, the transverse growth is now

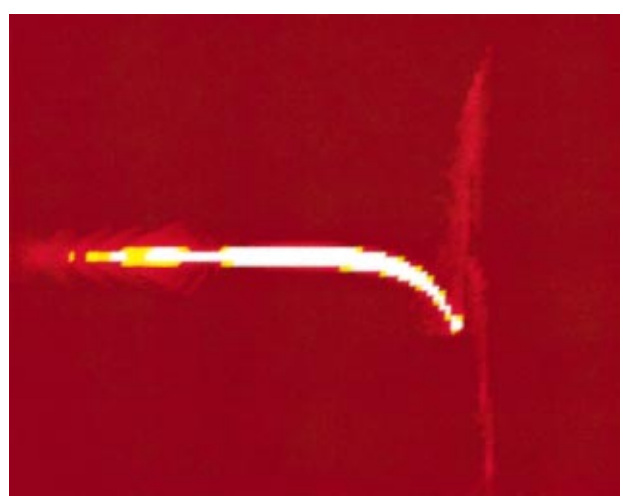

FIG. 10. (Color) The same beam as in Fig. 9, immediately downstream of the 1.5 m plasma. The color scale shown as in Fig. 9.

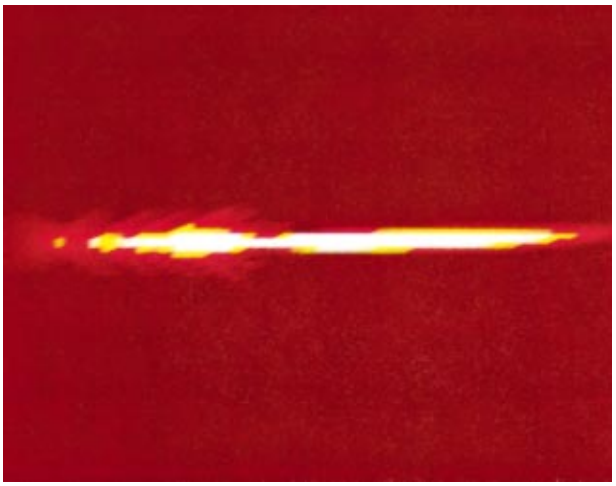

FIG. 11. (Color) The same beam as in Fig. 9, with σ_z half its value in Table I, immediately downstream of the 1.5 m plasma. Horizontal and vertical dimensions are 2.1 and 1.5 mm, respectively.

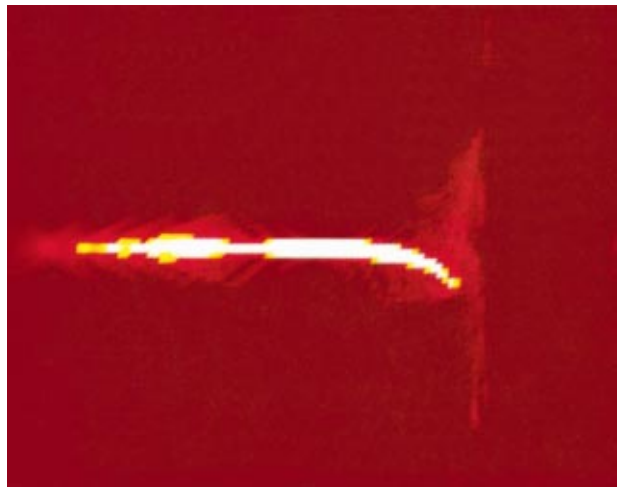

FIG. 13. (Color) The same beam as in Fig. 9, with N_b half its value in Table I, immediately downstream of the 1.5 m plasma. Horizontal and vertical dimensions are 4.2 and 1.5 mm, respectively.

only slighly reduced, as compared with Fig. 10. The transverse effects are less senstive to beam charge than to bunch length and plasma frequency for ranges of parameters close to those of Table I.

IV. INTEGRATED AND TIME-RESOLVED DIAGNOSTICS

In this section we provide a survey and analysis of an illustrative PWFA experimental setup, to indicate the primary considerations involved, and to translate the foregoing analysis into the observational features of transverse beam dynamics. The general beamline layout is shown in Fig. 14. The dispersion produced in the bending magnet ideally allows measurement of beam energy variations induced in the plasma. The drive beam exits the linear accelerator with some nominal variation in beam centroid transverse displacement (dipole perturbations) longitudinally along the beam. Such head–tail offset is typical for linear accelerators[31] due to wakefield-induced kicks of the beam tail. Transverse wakefields in the plasma amplify and distort incoming beam head–tail offsets, leading to beam breakup and deflection.

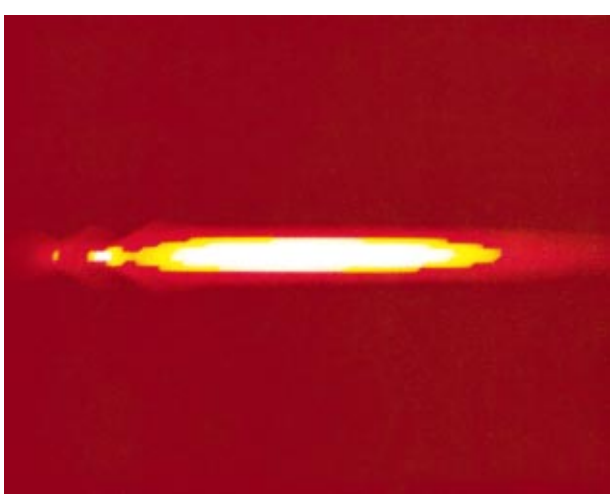

FIG. 12. (Color) The same beam as in Fig. 9, with k_p half its value in Table I, immediately downstream of the 1.5 m plasma. Horizontal and vertical dimensions are 4.2 and 1.5 mm, respectively.

A. Orbit simulations

In general, absent beam–plasma interaction, the electron beam orbit as observed with the help of BPMs, will fit to a superposition of sine-like, cosine-like, and dispersive rays. With plasma turned on, the beam orbit will exhibit a discontinuity across the plasma chamber, and based on optics characterization absent plasma, a deflection angle may be inferred. Thus, the first useful result of theoretical wakefield studies is to provide some estimate of angular deflection versus incoming beam head–tail tilt. To make a comparison between theory and observation we form the charge-weighted average,

$$\langle f\rangle_s=\frac{1}{Q_b}\int_{-\infty}^{+\infty} d\tau I_b(\tau) f(s,\tau),$$

where quantities f of interest include ξ, ξ', as well as second moments.

For experimentally accessible parameters, we expect amplification of beam-tail jitter by $\approx$1–100$\times$. For a current-weighted centroid, the amplification is significantly less. Figure 15 shows the evolution of the current-weighted centroid as the PIC simulation indicates for parameters in Table II.

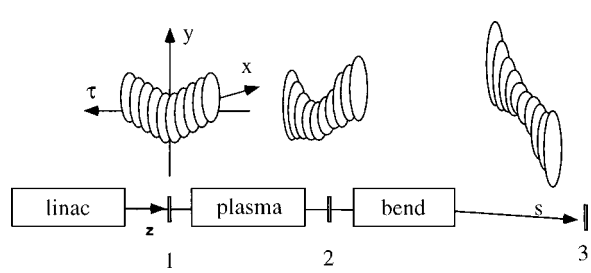

FIG. 14. Illustration of a PWFA experimental setup.

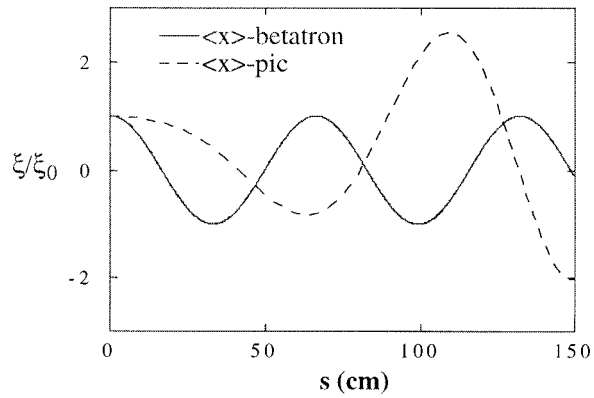

FIG. 15. PIC current-weighted centroid evolution. Betatron oscillation of an equilibrated channel, absent hosing, shown for reference.

For reference, the figure also includes betatron oscillations, as would be expected in an equilibrated ion-channel absent electron-hose instability.

Due to the strong focusing witnessed by the beam in plasma, we expect the beam trajectory upon leaving the plasma cell to be largely independent of initial transverse centroid angle $\langle \xi' \rangle$ and primarily dependent upon initial offset $\langle \xi \rangle$. Thus one is, in general, interested in plots of angle versus offset. For an ideal infinite plasma channel that has equilibrated to the beam we expect jitter in beam ''head–tail offset'' $\xi = \dot{\xi}_0 \tau$ to provide a variation of beam trajectory exit angles ξ' from the plasma tank. The width in this distribution of angles is, in turn, a function of plasma density, and can be calculated using the MAC and PIC simulations.

For illustration, the linearized MAC code is used to simulate the effect of initial head–tail offset on a final centroid trajectory angle for a variety of plasma densities using other beam and plasma parameters as in Table I. Figure 16 shows the kick strength x_b'/x_b as a function of plasma density. Experimentally one may compare the measured width in exit-angle distribution with the calculated dependence on plasma density, for example, with a random incoming distribution in head–tail offset parameter ξ_0'.

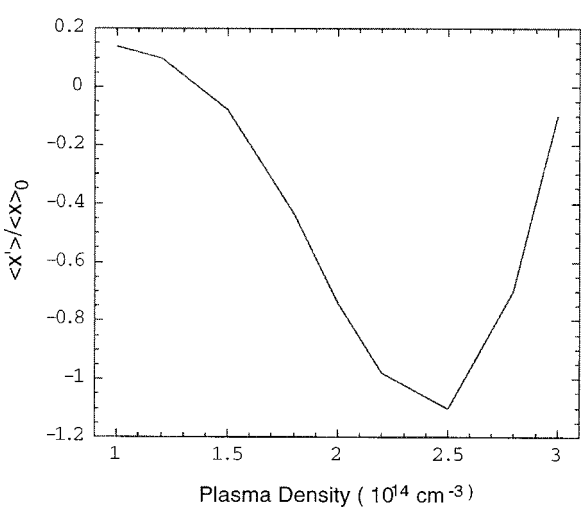

FIG. 16. MAC result for transverse average beam-centroid exit angle versus plasma density.

B. Lensing

A second generic set of diagnostics consists of beam profile monitors, either wire type, or radiator type.[32] In the following we indicate effects one may expect to observe in such images.

For a fixed length plasma cell, in the absence of wakefield effects, one expects the beam waist upon exit to undergo oscillations as a function of plasma density due to the betatron focusing of the ion channel. PIC results for parameters as in Table I differ due to scalloping occurring at the beam head and defocusing and deflection at the beam tail. For instance, for the plasma density in Table I, PIC simulation indicates a reduction in σ_x by 8% at the exit of the plasma tank, compared with the 89% expected assuming a pure-betatron focusing channel. Also, the PIC calculated variation of beam spot size with plasma density is less rapid than for the pure betatron channel. Experimentally, changes in the beam spot size can be measured by imaging the optical transition radiation both upstream and downstream of the plasma. These focusing effects, along with deflection effects, vary with plasma density and can be compared with the PIC results.

C. Transient diagnostics

A third category of diagnostic corresponds to those of the previous section, but observed via a streak camera to provide resolution along the very short time scale of a single bunch. In this section we discuss a particular interest in this diagnostic, namely distinguishing of betatron focusing versus wakefield amplification. The betatron focusing property of the ion channel formed by the beam head can, in principle, produce a deflection of the beam centroid much akin to a wakefield effect. The following experimental signatures, as evidenced in a time-resolved streak camera image, can distinguish this betatron focusing effect from the transverse wakefield growth. First, for a given incident beam profile, greater deflection of the beam centroid can occur with wakefield amplification than with purely betatron deflection. Second, beam ''hosing'' is expected with wakefield amplification and is not possible with purely betatron focusing. Hosing occurs when different longitudinal sections of the beam oscillate at different frequencies, leading to amplification and distortion of incoming dipole perturbations. In contrast, pure betatron focusing should result in all particles in the beam oscillating at a single betatron frequency.

It is not possible using projected transverse images to distinguish linear head–tail offset from increased spot size for a Gaussian beam. Therefore, as a more direct means to experimentally observe wakefield amplification and deflection, a streak camera set on a radiator immediately upstream of the plasma providing resolution along the bunch can be used to diagnose initial head–tail offset. This image can then be compared to time-resolved streaked images downstream of the plasma. Time-resolved centroid shifts can be measured and weighed against PIC results. Variation of deflection of

various regions of the beam tail with plasma density can also be measured and compared with PIC predictions. Also, by measuring the deflection of portions of the beam tail versus initial tail offset, it is possible, in principle, to experimentally distinguish between purely betatron versus wakefield deflection, as the latter can be greater by an order of magnitude, as shown in Sec. III.

V. CONCLUSIONS

PWFA experiments have the primary goal of demonstrating substantial beam energy gain via the longitudinal plasma wakefield. For recently proposed beam and plasma PWFA parameters,[4] transverse beam perturbations can easily dominate the problem. It is worth noting the respective scalings of transverse growth factor and accelerating gradient with bunch length, beam current, and plasma density. Adopting a linearized theory for the longitudial accelerating gradient, one has[4]

$$E_z \approx 4\pi e k_p^2 \int d\zeta' n_b(\zeta') \pi a^2 \cos k_p(\zeta - \zeta'), \tag{18}$$

where E_z is the electric field, and it is assumed that $k_p \sigma_{x,y} < 1$. We note that the amplitude of the electric field is roughly independent of spot size for this limit. Assuming a Gaussian longitudinal current profile, the peak longitudinal electric field at the beam tail can be approximated roughly by

$$E_z \approx 4\pi e^2 N_b k_p^2 \exp(-k_p^2 \sigma_z^2/2). \tag{19}$$

This form is strictly valid when $n_b < n_p$, not the case for the underdense regime. However, this approximate form is thought to be good within a factor of 2 or so for parameters of Table I, provided $N_b r_e / \sigma_z \ll 1$.[4] Examining Eq. (19) further, we note a linear scaling of E_z with the number of electrons per bunch, and a reduction for longer bunch lengths, σ_z greater than $\approx \lambda_p/4$, due to the diminished beam current Fourier component at the plasma frequency.

Meanwhile, the argument determining exponential growth of transverse head–tail offset is *independent* of the number of electrons per bunch, in the underdense limit, as seen in Eq. (12). Thus, the longitudinal accelerating gradient can be increased linearly with N_b without causing increased transverse-wakefield growth, at a fixed bunch length. Further, at fixed plasma density, it is possible to decrease transverse growth and increase acceleration by reducing the bunch length. Both longitudinal and transverse wakefield effects grow with increased plasma density, except the longitudinal effect wanes once $\sigma_z > \lambda_p/4$. The transverse electron-hose instability continues to grow with increasing plasma density. The PIC simulation indicates that for parameters of order as in Table I, it is possible to limit the bunch tail deflection associated with the nonlinear collapse of the ion channel by respecting $k_p \sigma_z < 1$.

In this paper we have for the first time provided an extensive parameter survey, along with associated scalings, for unstable transverse perturbations arising in recently proposed underdense PWFA schemes. In addition, we have provided a framework that illustrates how these transverse wakefield effects can be quantified experimentally.

ACKNOWLEDGMENTS

We are grateful to Johnathan Wurtele, Eric Esarey, Wim Leemans, Palma Catravas, and Max Zolotorev for their helpful remarks. We thank Angie Seymour for her support.

This work was supported by the U.S. Department of Energy under Contract No. DE-AC03-76SF00515.

[1] P. Chen, J. M. Dawson, R. W. Huff, and T. Katsouleas, Phys. Rev. Lett. **54**, 693 (1985).
[2] J. Krall and G. Joyce, Phys. Plasmas **2**, 1326 (1995).
[3] N. Barov, M. E. Conde, W. Gai, and J. B. Rosenzweig, Phys. Rev. Lett. **80**, 81 (1998).
[4] R. Assmann *et al.*, ''Progress toward E-157: A 1 GeV plasma wakefield accelerator,'' *Proceedings of the 1999 Particle Accelerator Conference* (The Institute of Electrical and Electronics Engineers, Inc., New York, in press).
[5] T. Katsouleas, Phys. Rev. A **33**, 2056 (1986).
[6] S. Wilks, T. Katsouleas, J. M. Dawson, P. Chen, and J. J. Su, IEEE Trans. Plasma Sci. **PS-15**, 210 (1987).
[7] J. B. Rosenzweig, Phys. Rev. A **38**, 3634 (1988).
[8] T. Katsouleas and W. B. Mori, Phys. Rev. Lett. **61**, 90 (1988).
[9] J. Krall, G. Joyce, and E. Esarey, Phys. Rev. A **44**, 6854 (1991).
[10] J. B. Rosenzweig, D. B. Cline, B. Cole, H. Figueroa, W. Gai, R. Konecny, J. Norem, P. Schoessow, and J. Simpson, Phys. Rev. Lett. **61**, 98 (1988).
[11] J. B. Rosenzweig, P. Schoessow, B. Cole, W. Gai, R. Konecny, J. Norem, and J. Simpson, Phys. Rev. A **39**, 1586 (1989).
[12] J. B. Rosenzweig, P. Schoessow, B. Cole, C. Ho, W. Gai, R. Konecny, S. Mtingwa, J. Norem, M. Rosing, and J. Simpson, Phys. Fluids B **2**, 1376 (1990).
[13] R. Keinigs and M. E. Jones, Phys. Fluids **30**, 252 (1987).
[14] J. J. Su, T. Katsouleas, J. M. Dawson, P. Chen, M. Jones, and R. Keinigs, IEEE Trans. Plasma Sci. **PS-15**, 192 (1987).
[15] D. H. Whittum, Phys. Fluids B **4**, 476 (1992).
[16] J. B. Rosenzweig, B. Breizman, T. Katsouleas, and J. J. Su, Phys. Rev. A **44**, R6189 (1991).
[17] D. H. Whittum, W. M. Sharp, S. S. Yu, M. Lampe, and G. Joyce, Phys. Rev. Lett. **67**, 991 (1991).
[18] D. H. Whittum, M. Lampe, G. Joyce *et al.*, Phys. Rev. A **46**, 6684 (1992).
[19] M. Lampe, G. Joyce, and D. H. Whittum, Phys. Fluids B **5**, 1888 (1993).
[20] D. H. Whittum, Phys. Plasmas **4**, 1154 (1997).
[21] D. H. Whittum, A. M. Sessler, J. J. Stewart, and S. S. Yu, Part. Accel. **34**, 89 (1990).
[22] B. W. Montague and W. Schnell, in *Laser Acceleration of Particles*, edited by Chan Joshi and Thomas Katsouleas, AIP Conf. Proc. **130** (American Institute of Physics, Woodbury, New York, 1985), p. 146.
[23] D. P. Murphy, M. Raleigh, R. E. Pechacek, and J. R. Grieg, Phys. Fluids **30**, 232 (1987).
[24] A. E. S. Green, Radiat. Res. **64**, 119 (1975); A. E. S. Green and T. Sawada, J. Atmos. Terr. Phys. **34**, 1719 (1972).
[25] P. Felsenthal and J. M. Proud, Phys. Rev. **139**, 1796 (1965).
[26] M. Mitchner and C. H. Kruger, Jr., *Partially Ionized Gases* (Wiley, New York).
[27] F. J. Mehr and M. A. Biondi, Phys. Rev. **181**, 264 (1969).
[28] C. B. Schroeder, D. Whittum, and J. S. Wurtele, Phys. Rev. Lett. **82**, 1177 (1999).
[29] D. Whittum, ''Electron-hose instability in an annular plasma sheath,'' J. Phys. D **30**, 2958 (1997).
[30] R. C. Davidson, *Physics of Nonneutral Plasmas* (Addison-Wesley, Redwood City, 1990).
[31] J. Seeman, ''Observation of high current effects in high-energy linear accelerators,'' *Proceedings of the Joint US–CERN Particle Accelerator School: Frontiers of Particle Beams: Intensity Limitations*, edited by M. Dienes, M. Month, and S. Turner (Springer-Verlag, Berlin, 1992), p. 614.
[32] P. Catravas *et al.*, ''Beam profile measurement at 30 GeV using optical transition radiation,'' in Ref. 4.